Automated detection of exudates in colored retinal images for diagnosis of diabetic retinopathy

M. Usman Akram,* Anam Tariq, M. Almas Anjum, and M. Younus Javed

Computer Engineering Department, College of Electrical & Mechanical Engineering, National University of Sciences & Technology, Peshawar Road, Rawalpindi 46000, Pakistan

*Corresponding author: usmakram@gmail.com

Received 14 February 2012; revised 17 May 2012; accepted 20 May 2012; posted 29 May 2012 (Doc. ID 162860); published 9 July 2012

Medical image analysis is a very popular research area these days in which digital images are analyzed for the diagnosis and screening of different medical problems. Diabetic retinopathy (DR) is an eye disease caused by the increase of insulin in blood and may cause blindness. An automated system for early detection of DR can save a patient's vision and can also help the ophthalmologists in screening of DR. The background or nonproliferative DR contains four types of lesions, i.e., microaneurysms, hemorrhages, hard exudates, and soft exudates. This paper presents a method for detection and classification of exudates in colored retinal images. We present a novel technique that uses filter banks to extract the candidate regions for possible exudates. It eliminates the spurious exudate regions by removing the optic disc region. Then it applies a Bayesian classifier as a combination of Gaussian functions to detect exudate and nonexudate regions. The proposed system is evaluated and tested on publicly available retinal image databases using performance parameters such as sensitivity, specificity, and accuracy. We further compare our system with already proposed and published methods to show the validity of the proposed system.

OCIS codes: 100.0100, 100.5010, 100.2960, 100.2980.

1. Introduction

Diabetic retinopathy (DR) is a common eye disease that is caused due to increase of insulin in blood. It is one of the leading causes of blindness in industrialized countries [1]. DR is a progressive disease, but early detection and diagnosis of DR can save vision. Recent studies have shown that one out of five patients with newly discovered type II diabetes has DR at the time of diagnosis, whereas in the first five years after diagnosis of type I diabetes, DR almost never occurs [2].

The common symptoms of DR are blurred vision, floaters and flashes, and sudden loss of vision [2]. A healthy retina consists of different components: blood vessels, fovea, macula, and optic disc (OD) [3]. DR is broadly divided into two stages, i.e., nonproliferative DR (NPDR) and proliferative DR (PDR) [1]. NPDR, also known as background DR, contains the early signs of DR such as microaneurysms, hemorrhages, hard exudates, and soft exudates. PDR is the advance stage of DR, and new abnormal blood vessels appear in retina called neovascularization (NV). These new vessels can appear inside the OD or anywhere in the retina, known as NV in disc and NV elsewhere, respectively [1].

DR is a progressive disease in which diabetes weakens the blood vessel boundaries and causes the leakage of blood into the retina. Microaneurysms and dot hemorrhages are the first signs of DR, which appear in retina due to tiny leaks. They appear as tiny red spots and also known as red or dark lesions [3]. If the blood leakage contains fats and proteins along with water, they cause yellow spots known as hard exudates. In addition to this, small and thin blood vessels may close off, causing some patches of retina deprived of blood supply. These small fluffy white

1559-128X/12/204858-09$15.00/0

patches in the retina are called cotton wool spots or soft exudates [4]. Hard and soft exudates are also known as bright lesions. The appearance of exudate on the fundus surface decreases the vision, but if the accumulation of fats and proteins is in the central region of retina, this can lead to total blindness. This is known as macular edema, and it is the most threatening sign as it can significantly reduce vision [4]. Figure 1 shows the healthy retinal image and image with exudates.

The diagnosis and treatment of DR need examination of retinal images, and it is difficult for ophthalmologists due to mass screening. Computer-aided diagnostic systems for detection of DR can help physicians [5]. Automatic assessment for bright lesions of the retina requires the precise localization and segmentation of the OD from the retinal image so that suitable lesion extraction and processing may be performed. Several methods have been developed for bright lesions and OD segmentation, but visual inspection and evaluation by receiver operating characteristic analysis have shown that there is still room for improvement: human observers are significantly more accurate than the methods, which show flaws around the OD [6].

A number of automated systems for retinal image enhancement, component segmentation, and lesion detection have been proposed. A standard contrast stretching technique was applied by [5] for fundus image enhancement and noise reduction. Local and adaptive contrast enhancement techniques are used in [6–8] for equalizing uneven illumination in the intensity channel of retinal images as a preprocessing step. The OD generally appears as a bright circular or elliptic region on the fundus image, and it helps in detection of bright lesions. Any change in the shape, color, or depth of the OD is an indicator of various ophthalmic pathologies. Reza *et al.* [9] presented a fixed and variable threshold-based method for OD and exudate detection. Another system based on marker-controlled watershed transformation for OD and exudate segmentation was proposed by the same author [10]. In [11], an approximate location of the OD is estimated by searching for regions of high intensity, diversity of gradient directions and convergence of blood vessels. A method based on highest local variance was used by Sinthanayothin *et al.* [12] to locate the position of the OD. Hoover and Goldbaum [13] utilized the geometric relationship between the OD and main blood vessels and used a fuzzy voting mechanism to find the location of the OD.

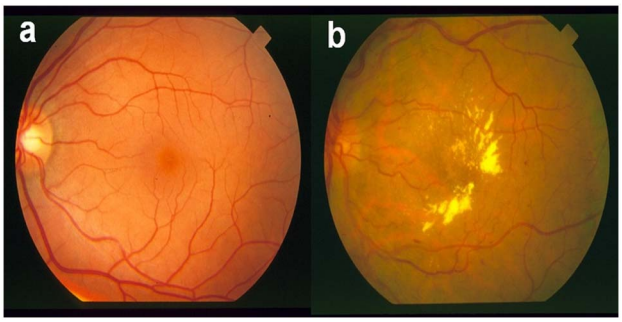

Fig. 1. (Color online) Retinal images: (a) healthy retinal image, (b) retinal image with exudates.

Sopharak *et al.* [14], [15] have used morphological reconstruction, fuzzy C mean (FCM), and support vector machines (SVMs) for exudate detection. The feature set consisted of cluster size, cluster intensity, number of edge pixels, neighborhood intensity, and difference of Gaussian. Osareh *et al.* [16] used a detailed feature set consisting of color, shape, size, and texture for exudate classification. They used a multilayer neural network classifier for this purpose. In [17] candidate regions for exudates were extracted using morphological closing of the luminance channel, local standard variation in a sliding window, and watershed transform. Wang *et al.* [18] proposed a system that combines a brightness adjustment procedure with a statistical classification method and local-window-based verification strategy for exudate detection. Another FCM-based method for OD and exudate detection was proposed by Yazid *et al.* [19]. Their system used the applications of FCM clustering, edge detection, Otsu thresholding, and inverse surface thresholding for this purpose. Acharya *et al.* [20] presented a higher-order spectra and SVM-based system for NPDR and PDR detection. They classified all three stages of NPDR with accuracies of 90%, 85%, and 70% for mild, moderate, and severe NPDR, respectively. A computer-aided system for classification of all NPDR lesions was proposed in [21]. They were able to identify dark lesions, hard exudates, and cotton wool spots with an accuracy of 82.6%, 82.6%, and 88.3%, respectively. Akram and Khan [22] presented a method for dark and bright lesion detection using a hybrid fuzzy-based classifier.

In this article, we present an automated system for detection of exudates in colored retinal images. It enhances the bright regions in an input retinal image using contrast enhancement and filter banks. The proposed method eliminates the false bright regions using OD segmentation and formulates the feature set for candidate exudate regions. A Gaussian mixture model is used to classify the candidate region as exudate and nonexudate. The proposed system is tested on three publicly available databases, i.e., STructured Analysis of the REtina (STARE), DiaretDB0, and DiaretDB1, and compared with already-published techniques.

This article consists of seven sections. Section 2 describes a brief overview of the proposed system followed by preprocessing and contrast enhancement in Section 3. Section 4 explains the candidate exudate region detection using the filter bank and eliminating the OD region. The feature set formation and classification of exudate and nonexudate regions are presented in Section 5. The results are presented in Section 6, followed by conclusions in Section 7.

2. System Overview

Systems based on digital image processing and machine learning are playing a vital role in biomedical research nowadays. Computer-aided diagnostic systems have brought new horizons in detection and treatment of many common diseases [3]. Similarly, analysis of digital retinal images is now being used for the detection and diagnosis of DR. Figure 2 shows a complete flow diagram for all phases of the proposed system starting from image acquisition to the classification of true exudate regions.

The proposed system uses image processing and machine learning techniques for the detection of exudates, a sign of DR, in retinal images. We divide the proposed system into three phases, i.e., retinal image acquisition and preprocessing, candidate exudate region detection and elimination of the OD, and finally feature set formulation and classification of regions as exudate and nonexudate regions. In candidate exudate detection, it enhances the contrast of all bright regions present in the retina and segments out possible candidate regions that can be classified as exudates. A Gaussian mixture model based on a Bayes decision rule is used to identify exudate and nonexudate pixels using a feature set of each region.

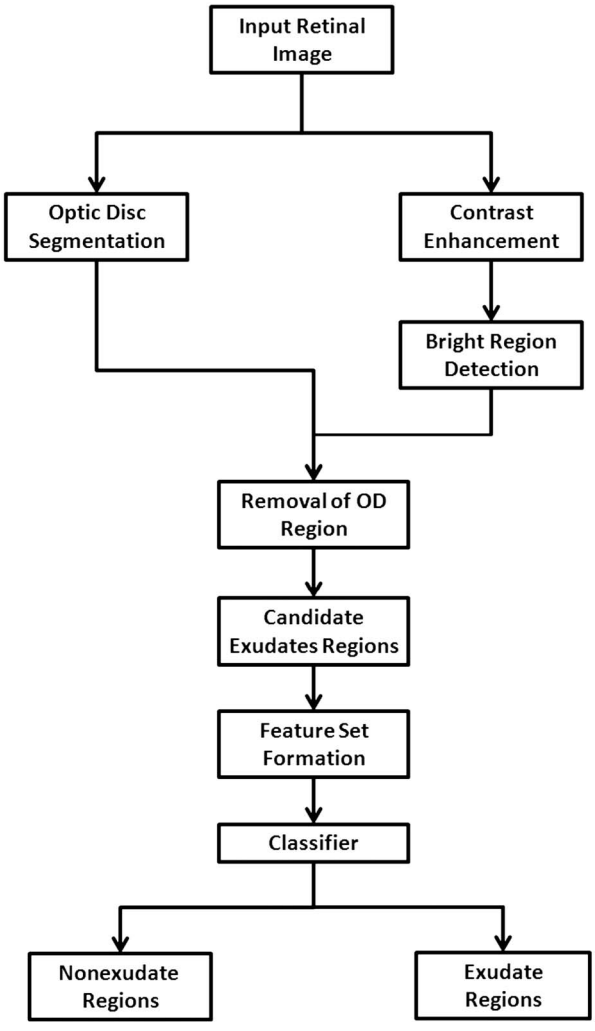

Fig. 2. Flow chart of proposed system.

3. Preprocessing and Contrast Enhancement

The purpose of preprocessing and contrast enhancement is to remove any false artifacts that occur during retinal image acquisition process.

A. Preprocessing

Preprocessing is done to remove the background and noise to enhance the quality of the input retinal image. In a computer-aided diagnostic system, the processing of the surrounding background and noisy areas is not necessary and consumes more processing time at all stages. The accuracy and time consumption can be improved by cropping out the background and noisy regions from the image. Noise in a color retinal image is normally due to noisy pixels and pixels whose colors are distorted cause of inadequate illumination. Since illumination is usually adequate in the center of the image, poor image quality regions are located near the edge of the retinal image. Regions with poor image quality may cause errors in abnormality detection. That is why they should be detected and removed before detection of abnormalities. We used a mean- and variance-based method for background estimation and hue, saturation, and intensity channels for noise removal. The detailed work of preprocessing the algorithm used in proposed system is explained in our previous system given in [23]. Figure 3 shows the output of preprocessing phase for an input retinal image.

B. Contrast Enhancement

Exudates, also known as bright lesions, appear as bright spots and patches in the fundus image with highest contrast in the green plane of the color image [17]. Ophthalmologists have no difficulty in identifying these lesions, but there are different factors, such as variability of image clarity, variation in image background texture, confusion with OD pixels, and presence of other lesions, which make identification difficult for automated systems.

An automated system for detection of exudates should enhance the contrast of bright regions with smoothing of dark regions. For exudate detection, morphological closing is used to smooth dark regions

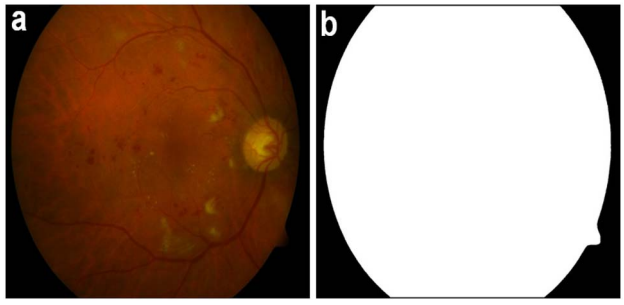

Fig. 3. (Color online) Preprocessing: (a) original retinal colored image, (b) preprocessing mask created using method defined in [23].

such as hemorrhages and blood vessels using Eq. (1) [17]:

$$\phi_f^{(sB)} = \min[\max f(x+b)]. \tag{1}$$

Here f is the preprocessed colored image and $b \in sB$, where sB represents the structuring element B with size s. This gives us a smooth fundus region ϕ_f containing bright regions only, but they need contrast enhancement. The objective of contrast enhancement is to improve the contrast of lesions for easy detection using a $w \times w$ sliding window with assumption that w is large enough to contain a statistically representative distribution of the local variation of lesions [12].

$$g = 255\frac{[\Phi_w(\phi_f) - \Phi_w(\phi_{f\min})]}{[\Phi_w(\phi_{f\max}) - \Phi_w(\phi_{f\min})]}, \tag{2}$$

where Φ_w is the sigmoid function for a window defined as

$$\Phi_w(\phi_f) = \left[1 + \exp\left(\frac{m_w - f}{\sigma_w}\right)\right]^{-1} \tag{3}$$

and $\phi_{f\max}$ and $\phi_{f\min}$ are maximum and minimum intensity value of smooth green channel image, respectively. m_w and σ_w are the mean and variance of intensity values within the window, respectively. Figure 4 shows the results of contrast enhancement.

4. Candidate Exudate Region Detection

The preprocessing and contrast enhancement stage removes all artifacts and enhances the contrast of bright lesions by suppressing and smoothing out all dark and red components present in the retinal image.

A. Filter Bank

The automated exudate detection method should detect as many regions as it can in the candidate region detection phase. In our system, we used the Gabor filter bank for detection of all possible bright regions. Gabor filters are famous due to their fine frequency tuning and orientation selectiveness. They are appropriate for texture representation and discrimination [24]. A Gabor filter is represented by a Gaussian kernel function, which can model a wide range of shapes depending upon values of its parameters [24]. This property makes them suitable for detection of exudates. Equation (4) describes the filter bank used in proposed system:

$$G_{\mathrm{FB}} = \frac{1}{\sqrt{\pi r}\sigma} e^{-\frac{1}{2}\left[\left(\frac{d_1}{\sigma}\right)^2 + \left(\frac{d_2}{r\sigma}\right)^2\right]}(d_1(\cos\Omega + \iota\sin\Omega)), \tag{4}$$

where σ, Ω, and r are the standard deviations of Gaussian, spatial frequency, and aspect ratio, respectively. θ is the orientation of filter, $d_1 = x\cos\theta + y\sin\theta$, and $d_2 = -x\sin\theta + y\cos\theta$. The contrast-enhanced image g is convolved with Gabor filter G centered at location (s,t) to generate Gabor filter response γ for selected values of σ, Ω, and θ, given in Eq. (5) [24]:

$$\gamma(\sigma,\Omega,\theta) = \sum_x \sum_y g(x,y) G_{\mathrm{FB}}(s-x, t-y, \sigma, \Omega, \theta, r). \tag{5}$$

For considered frequency and scale values, the maximum Gabor filter bank response $M_\gamma(\sigma,\Omega)$ is computed using Eq. (6) for θ spanning from 45° up to 180° at steps of 45°:

$$M_\gamma(\sigma,\Omega) = \max|\gamma(\sigma,\Omega,\theta)|. \tag{6}$$

The binary candidate regions for exudates are extracted from M_γ by applying a low adaptive threshold value T [25]. The threshold value is calculated such that it should extract all possible candidate lesion regions. Figure 5 shows the outputs of filter bank and adaptive thresholding technique.

B. OD Segmentation

The OD generally appears as a bright circular or elliptic region on the fundus image, and its exclusion is essential in achieving robust exudate detection. The regions segmented by thresholding of the filter-bank-based enhanced image also contain and OD region and pixels due to their similarity with exudates.

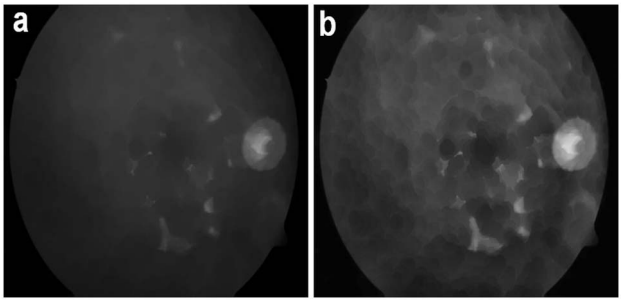

Fig. 4. Contrast enchantment: (a) smoothing of red components with mathematical morphological closing, (b) contrast-enhanced bright regions.

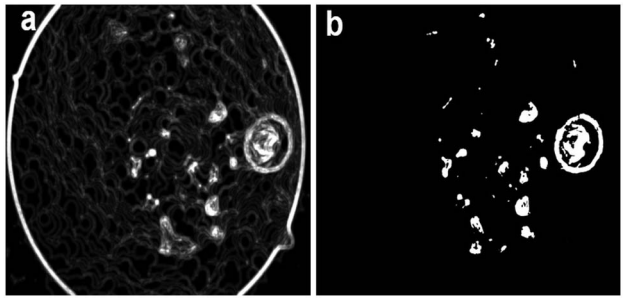

Fig. 5. Bright region detection: (a) enhanced bright regions using filter bank, (b) segmented bright regions using adaptive thresholding.

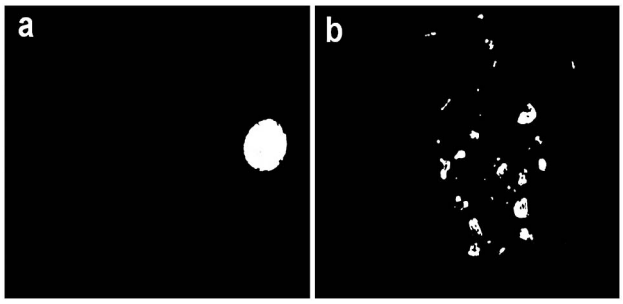

Fig. 6. Removal of OD region: (a) segmented OD using [26], (b) candidate exudate regions after elimination of spurious OD region.

For accurate detection exudates, these false and spurious pixels should be removed before the classification stage. The proposed system locates and segments the OD using image averaging and Hough transformation, respectively. The detailed work for OD segmentation is given in our previously proposed system [26]. Figure 6 illustrates the segmentation and removal of OD region.

5. Classification

The candidate exudate region detection phase extracts as many possible regions as it can for possible exudates. The threshold value is deliberately kept low so that not a single pixel containing exudate will be missed at that stage. We remove the spurious pixels or nonexudate regions in classification stage.

A. Feature Set Formulation

Exudates appear as bright yellow spots with variable size and shape but they have strong and sharp edges. The candidate exudate region extraction stage gives all possible regions that can be considered as potential exudates. If a retinal image χ contains k potential candidate regions, then the set representation for an image χ is $\chi = \{\upsilon_1, \upsilon_2, \upsilon_3, \cdots, \upsilon_k\}$. For an automated system to distinguish between exudate and nonexudate regions, a feature set is formed for each candidate region. Each object or candidate exudate region is considered as sample for classification and represented by a feature vector containing m features; i.e., for a sample candidate region υ from an image χ, the feature vector is $\upsilon = \{x_1, x_2, x_3, \cdots, x_m\}$. The description of features we used for classification of exudate and nonexudate regions are as follows:

Area (x_1) is the count of number of pixels in candidate exudate region and is defined as $A = \sum_{\upsilon_i} 1$ sum of all pixels in candidate region υ_i.
Compactness (x_2) is the measure of shape defined as $C = p^2/(4\pi A)$, where p and A are the perimeter length and area of candidate region, respectively.
Mean intensity (x_3) is the mean intensity value of the contrast-enhanced green channel for all pixels within the candidate region.
Mean hue (x_4), *mean saturation* (x_5), and *mean value* (x_6) for each candidate region are calculated in order to differentiate exudate and nonexudate regions on the basis of their color properties.
Mean gradient magnitude (x_7) for edge pixels is computed to differentiate between strong and blurry edges.
Entropy (x_8) is the value of all pixels in the square region including candidate region pixels and its neighboring pixels.
Energy (x_9) is calculated by summing the intensity values of all pixels within the candidate region and dividing it by total number of candidate region pixels.

B. Gaussian Mixture Model

In candidate lesion detection, the threshold value for lesion segmentation was deliberately kept low to ensure that as many lesions as possible would be detected. The spurious candidates will be removed in classification. In order to classify the candidate region as an exudate or nonexudate region, we use a Bayesian classifier using Gaussian functions known as the Gaussian Mixture Model (GMM) [27].

We define two classes such as $R_1 = \{\text{exudate region}\}$ and $R_2 = \{\text{nonexudate region}\}$. A supervised classification method is used for final classification by dividing the data set into training and testing subsets randomly. The classifier is trained using the training data set with labeled lesions, and we used the Bayes decision rule to obtain a decision rule based on estimates from the training set. The Bayes decision rule is stated as [28]

$$\begin{aligned} &\text{choose } R_1 \text{ if } p(\mathbf{v}|R_1)P(R_1) > p(\mathbf{v}|R_2)P(R_2), \\ &\quad \text{otherwise choose } R_2, \end{aligned} \tag{7}$$

where $p(\mathbf{v}|R_i)$ is the class conditional probability density function (pdf), also known as likelihood, and $P(R_i)$ is the prior probability of class R_i, which is calculated as the ratio of class R_i samples in the training set. The class conditional pdf of the feature vector for different classes is computed using multivariate Gaussian pdf [28]:

$$N(\mathbf{v}|\mu, \Sigma) = \frac{1}{(2\pi)^{\frac{m}{2}}|\Sigma|^2} \exp\left[\frac{-1}{2}(\mathbf{v}-\mu)\Sigma^{-1}(\mathbf{v}-\mu)\right], \tag{8}$$

where $\mathbf{v}$ and μ are the feature vector containing m number of features and the mean vector containing mean of each feature, respectively. Σ is a $m \times m$ covariance matrix. In our case, $m = 9$. We model the class conditional pdfs as a linear combination of weighted Gaussian functions to represent the likelihood of a GMM using Eq. (9):

$$p(\mathbf{v}|R_i) = \sum_{j=1}^{\kappa_i} N(\mathbf{v}|\mu_j, \Sigma_j)\omega_j, \tag{9}$$

where κ_i is the number of Gaussian mixtures used for Bayesian classification, $p(\mathbf{v}|R_i)$ is an m-dimensional Gaussian distribution of weight ω_j, and $R_i = \{R_1, R_2\}$ are the two classes used in proposed system.

Equations (8) and (9) show the likelihoods for a single Gaussian distribution and the GMM, respectively.

The GMM characterizes as a classifier having a halfway point between purely nonparametric and parametric models. It provides fast testing at the cost of a more expensive training phase. Although nonparametric techniques do not enforce any constraints on underlying data, they are still complex in computations. On the other hand, the GMM guarantees a fast testing stage independent of the number of training samples and depends only on the chosen value of κ.

We apply expectation maximization (EM) to search for an optimal value of κ that optimizes the accuracy of the GMM using different validation sets randomly extracted from classified training data. The EM is an iterative method that chooses the optimal value of κ by finding the local maximum value of the GMM pdf for training data. The EM finds such a value of κ for which mixture of κ weighted Gaussians can represent the data accurately.

The proposed system uses the EM with supervised leaning in which we use *a priori* knowledge to guide the training process. This supervised estimation has a benefit over unsupervised as in unsupervised; the EM expects the availability of a large number of data to estimate the parameters. EM learning for the GMM includes learning of mixture weights ω and parameters for different values of κ. It consists of two steps, i.e., estimation and maximization. In the first step, the EM estimates the probability of each point and which Gaussian has generated it, and in the second step, it modifies the parameters to maximize the likelihood of data.

The EM starts with initial values of parameters (μ, Σ) and weight w for each Gaussian. In estimation step, the EM computes the probability (P_E) of each point for each Gaussian using Eq. (10):

$$P_E(n,j) = \frac{w_j N(\upsilon_n|\mu_j, \Sigma_j)}{\sum_{i=1}^{\kappa} N(\upsilon_n|\mu_i, \Sigma_i)\omega_i}. \tag{10}$$

Here $P_E(n,j)$ represents the probability that the nth candidate region υ_n is generated from the jth Gaussian. We do this for all κ Gaussians and candidate regions. The second step is the maximization of likelihood by changing the parameters. The mean, covariance matrix, and weight for jth Gaussian are updated using estimated probabilities and are given in Eqs. (11), (12), and (13), respectively:

$$\mu_j = \frac{1}{\xi_j} \sum_{n=1}^{N_{\text{Total}}} P_E(n,j)\upsilon_n, \tag{11}$$

$$\Sigma_j = \frac{1}{\xi_j} \sum_{n=1}^{N_{\text{Total}}} P_E(n,j)(\upsilon_n - \mu_j)(\upsilon_n - \mu_j)^T, \tag{12}$$

$$\omega_j = \frac{\xi_j}{N_{\text{Total}}}, \tag{13}$$

where $\xi_j = \sum_{n=1}^{N_{\text{Total}}} P_E(n,j)$ and N_{Total} are the total number candidate regions.

6. Experimental Results

A. Material

We use three standard retinal image databases, which are publicly available for testing and evaluation of DR screening and diagnostic algorithms. The first data set is named STARE, which is developed by Hoover and Goldbaum for analysis of vascular structure [13]. It consists of retinal images with a resolution of 700×605 acquired using a TopCon TRV-50 fundus camera.

For more evaluation and comparison purposes, two more databases named DiaretDB0 [29] and DiaretDB1 [30] are used. DiaretDB0 contains 130 retinal images, of which 20 are normal; 110 contain different lesions of DR. DiaretDB1 consists of 89 images, of which only 5 are normal; others contain different lesions. These two databases contain images with resolution of 1500×1152 and of different qualities in terms of noise and illumination.

Two trained human graders created ground truths of manually labeled exudate regions for these databases, and we used them for evaluation purposes. Human graders marked 87 regions as exudates in STARE images and 710 and 571 regions in DiaretDB0 and DiaretDB1, respectively. We divided the manually labeled regions into two equal data sets, i.e. training and testing data sets. Figures 7 and 8 show the segmented exudate regions, using the proposed method, for DiaretDB and STARE databases, respectively.

B. Results

In this section, we provide a quantitative evaluation and comparison of the proposed system for exudate detection. We also demonstrate the effectiveness of the proposed approach using the GMM to enhance the classification accuracy of exudates. We divided the databases into three sets of training and testing, containing regions from STARE, DiaretDB0, and DiaretDB1, respectively. Feature vector representation of regions from training data is generated as specified in Section 5 and is used to generate models required by the GMM to formulate a decision rule.

The performance of the proposed system is measured using sensitivity, specificity, positive predictive value (PPV), and accuracy as figures of merit. Sensitivity is a true positive rate, and specificity is a true negative rate. These parameters are calculated using Eqs. (14), (15), (16), and (17), respectively:

$$\text{sensitivity} = \frac{T_P}{(T_P + F_N)}, \tag{14}$$

$$\text{specificity} = \frac{T_N}{(T_N + F_P)}, \tag{15}$$

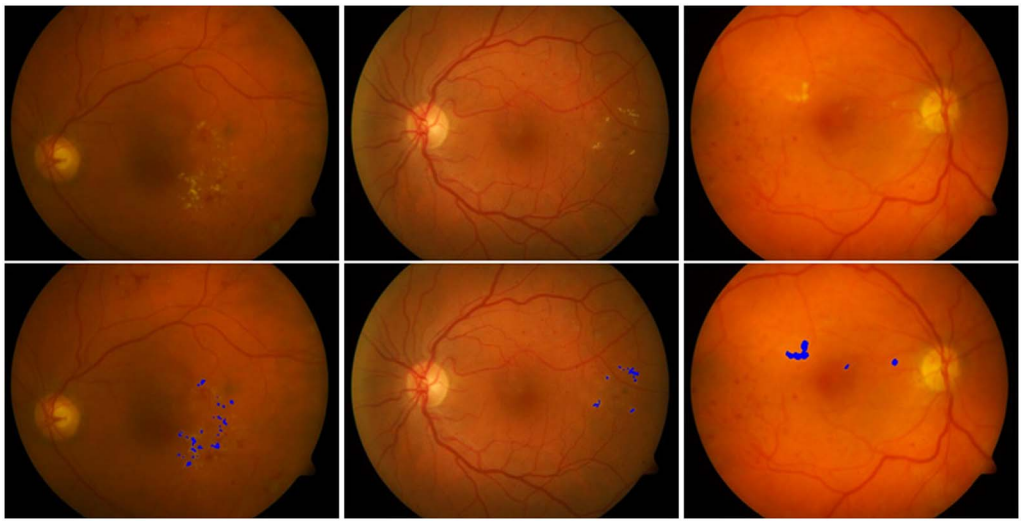

Fig. 7. (Color online) Exudate detection results for proposed method using three images from the DiaretDb0 and DiaretDB1 databases: (top) input retinal images, (bottom) detected exudates highlighted with blue color on the image.

$$\mathrm{PPV} = \frac{T_P}{(T_P + F_P)}, \tag{16}$$

$$\mathrm{accuracy} = \frac{(T_P + T_N)}{(T_P + T_N + F_P + F_N)}, \tag{17}$$

where

- T_P are true positives, meaning exudate regions are correctly classified.
- T_N are true negatives, meaning nonexudate regions are correctly classified.
- F_P are false positives, meaning nonexudate regions are wrongly classified as exudate regions.
- F_N are false negatives, meaning exudate regions are wrongly classified as nonexudate regions.

The experiments are performed by varying the number of Gaussian mixtures in the training phase for modeling of likelihoods and checking the corresponding accuracies. The performance of the proposed system is measured using the above-mentioned parameters and summarized in Table 1. The values for T_p, T_N, F_p, and F_N are calculated for the proposed system by comparing the test results with manually labeled ground truth data.

It is clear from the table that the proposed method has the best results for the DiaretDB1 database and the worst for the STARE database, the reasons being that the DIARETDB databases contain more training samples as compared to STARE and that there is much difference in the resolution and intensity variation of the DIARETDB and STARE databases. The training of the GMM has more contributions

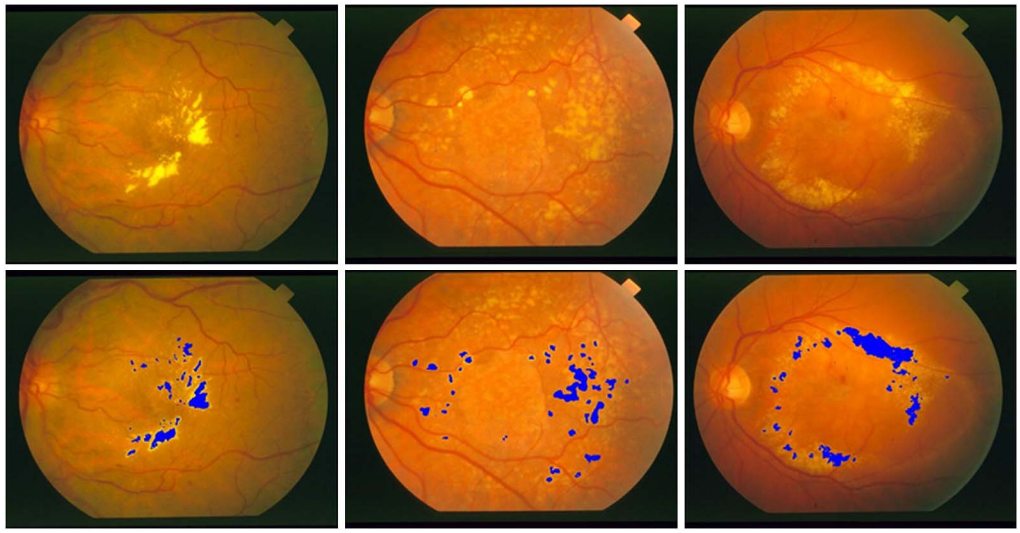

Fig. 8. (Color online) Exudate detection results for proposed method using three images from the STARE database: (top) input retinal images, (bottom) detected exudates highlighted with blue color on the image.

Table 1. Performance Evaluation of Proposed Method

Database	T_p	T_N	F_p	F_N	Sensitivity	Specificity	PPV	Accuracy
STARE	43	50	2	1	97.72	96.15	96.9	95.56
DiaretDB0	357	548	9	24	93.7	98.38	97.54	96.48
DiaretDB1	288	357	6	1	99.65	98.35	97.96	98.92
Combined	**688**	**955**	**17**	**26**	**96.36**	**98.25**	**97.45**	**97.59**

Table 2. Performance Comparison of Exudate Segmentation

Method	Sensitivity	Specificity	PPV	Accuracy
Sinthanayothin *et al.* [12]	88.5	99.7	—	—
Wang *et al.* [18]	—	70	—	100
Walter *et al.* [17]	92.74	100	92.39	—
Reza *et al.* [9]	96.7	100	94.9	—
Osareh *et al.* [16]	93	94.1	—	93.4
Yazid *et al.* [19]	94.25	99.2	78.65	—
Akram and Khan [22]	—	—	—	94.73
PM $\kappa = 3$	92.45	93.72	93.04	93.87
PM $\kappa = 10$	95.27	97.68	96.91	96.89
PM $\kappa = 12$	**96.36**	**98.25**	**97.45**	**97.59**
PM $\kappa = 18$	96.59	98.75	97.79	98.02

from DIARETDB, so their performance is high as compared to STARE.

For performance comparisons, we present the values of sensitivity, specificity, PPV, and accuracies of the methods of Sinthanayothin *et al.* [12], Wang *et al.* [18], Walter *et al.* [17], Reza *et al.* [9], Osareh *et al.* [16], Yazid *et al.* [19], and Akram and Khan [22]. Table 2 shows the performance comparison of the proposed method (PM) with these methods.

It is also demonstrated from Table 2 that the performance of the GMM increases as we increase the number of mixtures κ. It is important to note that the training process for the GMMs is computationally more expensive as we increase the value of κ, but it can be done offline. There was a little bit of improvement in the performance for $\kappa > 12$ as compared to training time because the GMM has a computation complexity of $O(n * \kappa)$, where n is number of classes. So we have calculated all the performance parameters for $\kappa = 12$.

The STARE database has been used by a number of authors to represent the performance of exudate detection; that is why we perform separate comparison results for the STARE database only with recently published methods such as Reza *et al.* [10] and Yazid *et al.* [19]. Table 3 shows the performance comparison of exudate segmentation for the STARE database in terms of sensitivity, specificity, and PPV. The table shows that the proposed system outperforms others especially in terms of PPV. This improvement is supported by accurate lesion detection stage and causing lower number of false positives due to removal of spurious regions, especially OD pixels. Another reason for improvement is the use of a detailed feature set and classifier for detection of exudates, which are not used by the above-mentioned authors.

Table 3. Performance Comparison of Exudate Segmentation for STARE Database

Method	Sensitivity	Specificity	PPV
Reza *et al.* [10]	63.6	98.6	79
Yazid *et al.* [19]	97.8	99	83.3
PM	**97.72**	**96.15**	**95.56**

7. Discussion and Conclusions

In this article, we presented a method for exudate detection in a colored retinal image. The proposed system consisted of three phases: preprocessing and image enhancement, candidate exudate region detection, and feature set formulation and classification. The bright regions are enhanced and a segmented using filter bank and adaptive thresholding, but they contained spurious regions, which we eliminated by removing the OD pixels.

The feature set for each candidate region is formed using different properties of exudates such as color, shape, and statistics. To improve the accuracy of exudate detection, we further implemented a Bayesian classifier as a linear combination of GMMs. The classifier divides the regions into two classes: exudate and nonexudate regions. We used GMMs as they represent a halfway between parametric and pure nonparametric models, providing a fast classification stage. The GMM requires a computationally extensive training phase using EM, but this can be traded off with fast classification stage and high accuracies.

We have used sensitivity, specificity, PPV, and accuracy parameters for evaluation purposes. The proposed system achieved values of 96.36%, 98.25%, 97.45%, and 97.59% for sensitivity, specificity, PPV, and accuracy, respectively, which are better than recently published methods. It is clear from the comparison that the proposed system has detected the

exudates with good accuracy and has outperformed previously proposed systems.

The performance is improved using the PM due to our emphasis on every stage of the system, for example the removal of OD pixels to reduce the number of false regions, use of sound feature sets with the help of good descriptors, and finally a reliable GMM-based classifier. The results demonstrated that the proposed system can be used in a computer-aided diagnostic system for DR as it identified and detected exudates with high accuracies.

References

1. E. M. Kohner, S. J. Aldington, I. M. Stratton, S. E. Manley, R. R. Holman, D. R. Matthews, and R. C. Turner, "United Kingdom prospective diabetes study, 30: diabetic retinopathy at diagnosis of noninsulin-dependent diabetes mellitus and associated risk factors," Arch. Ophthalmol. **116**, 297–303 (1998).
2. A. F. Amos, D. J. McCarty, and P. Zimmet, "The rising global burden of diabetes and its complications: estimates and projections to the year 2010," Diabet. Med. **14**, S7–S85 (1997).
3. A. Molven, M. Ringdal, A. M. Nordbo, H. Raeder, J. Stoy, G. M. Lipkind, D. F. Steiner, L. H. Philipson, I. Bergmann, D. Aarskog, D. E. Undlien, G. Joner, O. Sovik, G. I. Bell, and P. R. Njolstad, "Mutations in the insulin gene can cause MODY and autoantibody-negative type 1 diabetes," Diabetes **57**, 1131–1135 (2008).
4. R. N. Frank, "Diabetic retinopathy," Prog. Retinal Eye Res. **14**, 361–392 (1995).
5. S. C. Lee, E. T. Lee, R. M. Kingsley, Y. Wang, D. Russell, R. Klein, and A. Warn, "Comparison of diagnosis of early retinal lesions of diabetic retinopathy between a computer system and human experts," Arch. Ophthalmol. **119**, 509–515 (2001).
6. D. Usher, M. Dumskyj, M. Himaga, T. H. Williamson, S. Nussey, and J. Boyce, "Automated detection of diabetic retinopathy in digital retinal images: a tool for diabetic retinopathy screening," Diabet. Med. **21**, 84–90 (2004).
7. C. Sinthanayothin, V. Kongbunkiat, S. Phoojaruenchanachain, and A. Singlavanija, "Automated screening system for diabetic retinopathy," in *Proceedings of the 3rd International Symposium on Image and Signal Processing and Analysis* (IEEE, 2003), pp. 915–920.
8. A. Osareh, M. Mirmehdi, B. Thomas, and R. Markham, "Classification and localisation of diabetic-related eye disease," in *Proceedings of the 7th European Conference on Computer Vision*, Lecture Notes in Computer Science 2353 (Springer, 2002), pp. 502–516.
9. A. W. Reza, C. Eswaran, and S. Hati, "Automatic tracing of optic disc and exudates from color fundus images using fixed and variable thresholds," J. Med. Syst. **33**, 73–80 (2009).
10. A. W. Reza, C. Eswaran, and K. Dimyati, "Diagnosis of diabetic retinopathy: automatic extraction of optic disc and exudates from retinal images using marker-controlled watershed transformation," J. Med. Syst. **35**, 1491–1501 (2011).
11. H. Narasimha-Iyer, A. Can, B. Roysam, C. V. Stewart, H. L. Tanenbaum, A. Majerovics, and H. Singh, "Robust detection and classification of longitudinal changes in color retinal fundus images for monitoring diabetic retinopathy," IEEE Trans. Biomed. Eng. **53**, 1084–1098 (2006).
12. C. Sinthanayothin, J. A. Boyce, H. L. Cook, and T. H. Williamson, "Automated localisation of the optic disc, fovea, and retinal blood vessels from digital colour fundus images," Br. J. Ophthalmol. **83**, 902–910 (1999).
13. A. Hoover and M. Goldbaum, "Locating the optic nerve in a retinal image using the fuzzy convergence of the blood vessels," IEEE Trans. Med. Imag. **22**, 951–958 (2003).
14. A. Sopharak, B. Uyyanonvara, S. Barman, S. Vongkittirux, and N. Wongkamchang, "Fine exudate detection using morphological reconstruction enhancement," Int. J. Appl. Biomed. Eng. **1**, 45–50 (2010).
15. A. Sopharak, M. N. Dailey, B. Uyyanonvara, S. Barman, T. Williamson, K. T. Nwe, and Y. A. Moe, "Machine learning approach to automatic exudate detection in retinal images from diabetic patients," J. Mod. Opt. **57**, 124–135 (2010).
16. A. Osareh, B. Shadgar, and R. Markham, "A computational-intelligence-based approach for detection of exudates in diabetic retinopathy images," IEEE Trans. Inf. Technol. Biomed. **13**, 535–545 (2009).
17. T. Walter, J. C. Klein, P. Massin, and A. Erginay, "A contribution of image processing to the diagnosis of diabetic retinopathy detection of exudates in color fundus images of the human retina," IEEE Trans. Med. Imag. **21**, 1236–1243 (2002).
18. H. Wang, W. Hsu, K. Goh, and M. Lee, "An effective approach to detect lesions in colour retinal images," in *Proceedings of the IEEE Conference on Computer Vision and Pattern Recognition* (IEEE, 2000), Vol. 2, pp. 181–187.
19. H. Yazid, H. Arof, and H. M. Isa, "Automated identification of exudates and optic disc based on inverse surface thresholding," J. Med. Syst. **36**, 1997–2004 (2012).
20. U. R. Acharya, K. C. Chua, E. Y. K. Ng, W. Wei, and C. Chee, "Application of higher order spectra for the identification of diabetes retinopathy stages," J. Med. Syst. **32**, 431–488 (2008).
21. S. C. Lee, E. T. Lee, Y. Wang, R. Klein, R. M. Kingsley, and A. Warn, "Computer classification of nonproliferative diabetic retinopathy," Arch. Ophthalmol. **123**, 759–764 (2005).
22. M. U. Akram and S. A. Khan, "Automated detection of dark and bright lesions in retinal images for early detection of diabetic retinopathy," J. Med. Syst., doi:10.1007/s10916-011-9802-2 (2011).
23. A. Tariq and M. U. Akram, "An automated system for colored retinal image background and noise segmentation," in *2010 IEEE Symposium on Industrial Electronics and Applications (ISIEA)* (IEEE, 2010), pp. 405–409.
24. J. Sung, S. Y. Bang, and S. Choi, "A Bayesian network classifier and hierarchical Gabor features for handwritten numeral recognition," Pattern Recogn. Lett. **27**, 66–75 (2006).
25. R. C. Gonzalez and R. E. Woods, *Digital Image Processing*, 2nd ed. (Prentice-Hall, 2002).
26. M. U. Akram, A. Khan, K. Iqbal, and W. H. Butt, "Retinal image: optic disk localization and detection," *Image Analysis and Recognition*, Lecture Notes in Computer Science 6112 (Springer, 2010), pp. 40–49.
27. S. Theodoridis and K. Koutroumbas, *Pattern Recognition*, 1st ed. (Academic, 1999).
28. R. O. Duda, P. E. Hart, and D. G. Stork, *Pattern Classification* (Wiley, 2001).
29. T. Kauppi, V. Kalesnykiene, J. K. Kamarainen, L. Lensu, I. Sorri, H. Uusitalo, H. Klviinen, and J. Pietil, "DIARETDB0: evaluation database and methodology for diabetic retinopathy algorithms," Tech. Rep. (2005).
30. T. Kauppi, V. Kalesnykiene, J.-K. Kamarainen, L. Lensu, I. Sorri, A. Raninen, R. Voutilainen, H. Uusitalo, H. Klviinen, and J. Pietil, "DIARETDB1 diabetic retinopathy database and evaluation protocol," Tech. Rep. (2006).